RESEARCH ARTICLE

Engineering of molybdenum-cofactor-dependent nitrate assimilation in *Yarrowia lipolytica*

Thomas Perli[1,†], Irina Borodina[2,‡] and Jean-Marc Daran[1,*,§]

[1]Department of Biotechnology, Delft University of Technology, Van der Maasweg 9, 2629 HZ, Delft, The Netherlands and [2]The Novo Nordisk Foundation Center for Biosustainability, Technical University of Denmark, Kemitorvet, Building 220, 2800 Kgs. Lyngby, Denmark

[*]**Corresponding author:** Department of Biotechnology, Delft University of Technology, Van der Maasweg 9, 2629 HZ, Delft, The Netherlands. Tel: +31-15-27-82412; E-mail: J.G.Daran@TUDelft.nl

One sentence summary: This study establishes Molybdenum cofactor biosynthesis in *Yarrowia lipolytica* to expand the nutrient range thereof.

Editor: Zongbao Zhao
[†]Thomas Perli, http://orcid.org/0000-0002-4910-3292
[‡]Irina Borodina, http://orcid.org/0000-0002-8452-1393
[§]Jean-Marc Daran, http://orcid.org/0000-0003-3136-8193

ABSTRACT

Engineering a new metabolic function in a microbial host can be limited by the availability of the relevant cofactor. For instance, in *Yarrowia lipolytica*, the expression of a functional nitrate reductase is precluded by the absence of molybdenum cofactor (Moco) biosynthesis. In this study, we demonstrated that the *Ogataea parapolymorpha* Moco biosynthesis pathway combined with the expression of a high affinity molybdate transporter could lead to the synthesis of Moco in *Y. lipolytica*. The functionality of Moco was demonstrated by expression of an active Moco-dependent nitrate assimilation pathway from the same yeast donor, *O. parapolymorpha*. In addition to 11 heterologous genes, fast growth on nitrate required adaptive laboratory evolution which, resulted in up to 100-fold increase in nitrate reductase activity and in up to 4-fold increase in growth rate, reaching 0.13h^{-1}. Genome sequencing of evolved isolates revealed the presence of a limited number of non-synonymous mutations or small insertions/deletions in annotated coding sequences. This study that builds up on a previous work establishing Moco synthesis in *S. cerevisiae* demonstrated that the Moco pathway could be successfully transferred in very distant yeasts and, potentially, to any other genera, which would enable the expression of new enzyme families and expand the nutrient range used by industrial yeasts.

Keywords: molybdenum cofactor; nitrate reductase; nitrate assimilation; *Yarrowia lipolytica*; metabolic engineering

INTRODUCTION

As *Saccharomyces cerevisiae*, the Dipodascaceae yeast *Yarrowia lipolytica* has gained interest as a model yeast for dimorphism studies and as an industrial work horse (Barth and Gaillardin 1997). This strictly aerobic oleaginous Saccharomycetales yeast has been traditionally exploited for its ability to efficiently degrade a wide variety of abundant and cheap hydrophobic substrates such as *n*-alkanes, fatty acids and oils that was coupled to its remarkable high enzyme secretion capacity and production of organic acids such as citric and α-ketoglutaric acids (Tsugawa *et al.* 1969).

The fast development of dedicated molecular tools including the addition of CRISPR technology, enabled to propel *Y. lipolytica* as a potential contender of *S. cerevisiae* for the biosynthesis of commodity and speciality chemicals. *Y. lipolytica* has become

a reliable platform for metabolic engineering as illustrated by the synthesis of flavor compounds (Marella *et al.* 2020), insect sex pheromones (Holkenbrink *et al.* 2020), non-caloric sweeteners (Rumelhard *et al.* 2016), itaconic acid (Blazeck *et al.* 2015) and terpenoids (Arnesen *et al.* 2020) as a few examples.

Engineering *of Y. lipolytica* with increasingly more complex pathways will require the expression of an even broader range of enzymes as its attractiveness as metabolic engineering platform grows. Many enzyme activities require the presence of one or more essential cofactors (Broderick 2001; Champe, Harvey and Ferrier 2005). Therefore, the successful expansion of the enzyme repertoire in a microbial host may require the parallel broadening of its cofactor set. Whenever a cofactor requirement cannot be met by media supplementation because either (1) the cofactor is not commercially available or too expensive, (2) is unstable or (3) cannot be imported by the organism, metabolic engineering is required to enable its *de novo* biosynthesis or its transport. This approach was successful in the model yeast *Saccharomyces cerevisiae* as exemplified with the implementation of high affinity Ni^{2+} transport, an inorganic cofactor of Ni-dependent urease (Milne *et al.* 2015), or with the engineering of tetrahydrobiopterin pathway, that was instrumental in the implementation of *de novo* biosynthesis of opioids (Galanie *et al.* 2015; Li and Smolke 2016) and melatonin (Germann *et al.* 2016). More recently, the molybdenum cofactor biosynthesis pathway from the methylotrophic yeast *Ogataea parapolymorpha* was introduced in *S. cerevisiae* allowing expression of a functional Moco-dependent nitrate reductase that could support growth on media containing nitrate as sole nitrogen source (Perli *et al.* 2021). Although these pioneering studies demonstrated how metabolic landscape could be expanded beyond the natural ability of a microorganism, these approaches have not yet been transposed in other industrially relevant yeast species. Enabling Moco biosynthesis and nitrate assimilation in a evolutionarily distant yeast such as *Y. lipolytica* would confirm that the selected gene-set may be used in wide range of yeast species but would also contribute to further expand the metabolic capabilities of this microbial cell factory. Previous research has shown how *Y. lipolitica* accumulates lipids in nitrogen starving conditions (Ratledge 2002). Introduction of a heterologous nitrogen assimilation pathway such as the nitrate assimilation pathways could be applied to mimic a nitrogen-starving condition without actually having to limit the amount of nitrogen in the media.

As *S. cerevisiae* and more than 75% of the Saccharomycotina yeast species, *Y. lipolytica* is not able to synthesize molybdopterin cofactor (Shen *et al.* 2018) which precludes the possibility to harness enzyme families of biotechnological relevance.

Moco-dependent enzymes encompass more than 30 different catalytic activities divided in three main families, based on the Moco variant they require (Cvetkovic *et al.* 2010; Hille, Hall and Basu 2014). Moco can be directly used as cofactor or modified by either sulfuration of the molybdate ion to form sulfurated Moco or, in prokaryotes, by the covalent attachment of either GDP or CDP to molydopterin (MTP) to form Bis(Molybdopterin Guanine Dinucleotide) Molybdenum Cofactor or MTP-cytosine dinucleotide cofactor, respectively. In a large majority, Moco-dependent enzymes catalyse oxido/reduction reactions, often involving oxygen and are implicated in nutrient e.g. carbon, nitrogen and sulfur cycles or in detoxification of growth-inhibiting compounds thanks to the redox versatility of the Mo atom (Hille 2002).

Moco is composed of a molybdate (MoO_4^{2-}) oxyanion coordinated by two sulfur atoms on MTP, a tricyclic pterin scaffold. Moco cannot be supplemented in the media since the molecule is too unstable due to its oxygen sensitivity (Fischer *et al.* 2006). For this reason, Moco is, in the majority of cases, *de novo* synthesized intracellularly. The Moco biosynthetic pathway is very well conserved and it has been extensively studied in both prokaryotes and eukaryotes (Rajagopalan and Johnson 1992; Iobbi-Nivol and Leimkuhler 2013; Mendel 2013). The first step, which takes place in the mitochondria of eukaryotic cells, is catalysed by the heterodimer Cnx1/Cnx2, that cyclizes GTP onto pyranopterin monophosphate (cPMP). The molecule is then exported to the cytosol through a yet uncharacterized transporter, and it is converted to MPT by action of the MPT synthase complex ($Cnx5_2/Cnx6_2$) which donates two sulfur atoms present on a conserved Cysteine residue in the Cnx5 protein. Cnx5 is then reloaded with sulfur via a sulfur mobilization route that includes the adenyltransferase Cnx4 and a cysteine desulfurase that is typically involved in iron–sulfur cluster biosynthesis and tRNA thiolation, Nfs1 (Leimkuhler, Buhning and Beilschmidt 2017). In the final step, molybdate is inserted in a two-steps reaction catalyzed by the multi-domain protein Cnx3 (Iobbi-Nivol and Leimkuhler 2013). Previous studies showed that the yeast *S. cerevisiae* lacks a high-affinity molybdate transport system and that it is able to import the oxyanion only with low affinity, unless a high affinity transporter such as *Cr*Mot1 from *Chlamydomonas reinhardtii* is expressed (Tejada-Jimenez *et al.* 2007; Perli *et al.* 2021).

The goals of this study were to investigate whether the heterologous Moco biosynthetic pathway from the nitrate-assimilating yeast *O. parapolymorpha* could be functionally engineered in *Y. lipolytica*, together with a Moco-dependent nitrate assimilation pathway. To this end, a total of 11 genes encompassing Moco biosynthesis, molybdate transport and nitrate reduction functions were introduced in the oleaginous yeast *Y. lipolytica* using CRISPR/Cas9 gene-editing technology. The engineered strain was then subjected to adaptive laboratory evolution (ALE) in synthetic media with nitrate as the sole nitrogen source to evolve a fast-growing population. After that, single cell lines were isolated, phenotyped on nitrate containing medium and characterized by whole-genome resequencing.

MATERIAL AND METHODS

Strains, media and maintenance

All strains used and constructed in this study are shown in Table 1. All *Y. lipolytica* strains were derived from the strain ST6512 (W29, MATa *ku70Δ::Spycas9-EcDsdAMX4*; Marella *et al.* 2020). Yeast strains were grown on either YP (10 g/L Bacto yeast extract and 20 g/L Bacto peptone) or SM medium (Verduyn *et al.* 1992) with either 5 g/L KNO_3, or 2.3 g/L urea (SM_{NO3} and SM_{urea}, respectively) as sole nitrogen source. In all SM media variants, 6.6 g/L K_2SO_4 was added as a source of sulfate (Solis-Escalante *et al.* 2013). YP or SM media were autoclaved at 121°C for 20 min. After sterilization, SM was supplemented with 1 mL/L of filter-sterilized vitamin solution as previously described (Verduyn *et al.* 1992). A concentrated glucose solution was autoclaved at 110°C for 20 min and then added to the YP and SM medium at a final concentration of 20 g/L, yielding SMD and YPD, respectively. 500-mL shake flasks containing 100 mL medium and 100-mL shake flasks containing 20 mL medium were incubated at 30°C and 200 rpm in an Innova Incubator (Brunswick Scientific, Edison, NJ). Solid media were prepared by adding 1.5% (w/v) Bacto agar and, where indicated, 250 mg/L nourseothricin or 250 mg/L hygromycin B. *Escherichia coli* strains were grown in LB (10 g/L

Table 1. Strains used in this study.

Name	Relevant genotype	Parental strain	Reference
ST6512	MATa ku70Δ::pTEF1-Spcas9-tTEF12::pGPD-EcdsdAMX4-tLIP2	W29, Y-63746 and ATTC-20460	Marella et al. (2020)
IMX2264	MATa ku70Δ::pTEF1-Spcas9-tTEF12::pGPD-EcdsdAMX4-tLIP2 E_4Δ::pTEFin-OpCNX1-tPEX10 pGPD-OpCNX2-tLIP2	ST6522	This study
IMX2265	MATa ku70Δ::pTEF1-Spcas9-tTEF12::pGPD-EcdsdAMX4-tLIP2 E_4Δ::pTEFin-OpCNX1-tPEX10 pGPD-OpCNX2-tLIP2 C_2Δ::pTEFin-OpNFS1-tPEX10	IMX2264	This study
IMX2266	MATa ku70Δ::pTEF1-Spcas9-tTEF12::pGPD-EcdsdAMX4-tLIP2 E_4Δ::pTEFin-OpCNX1-tPEX10 pGPD-OpCNX2-tLIP2 C_2Δ::pTEFin-OpNFS1-tPEX10 pGPD-OpCNX3-tLIP2 E_1Δ::pTEFin-OpCNX3-tPEX10 pGPD-CrMoT1.tLIP2	IMX2265	This study
IMX2267	MATa ku70Δ::pTEF1-Spcas9-tTEF12::pGPD-EcdsdAMX4-tLIP2 E_4Δ::pTEFin-OpCNX1-tPEX10 pGPD-OpCNX2-tLIP2 C_2Δ::pTEFin-OpNFS1-tPEX10 pGPD-OpCNX3-tLIP2 E_1Δ::pTEFin-OpCNX3-tPEX10 pGPD-CrMoT1.tLIP2 C_3Δ::pTEFin-OpYNR1-tPEX10 pGPD-OpYNT1.tLIP2 pTEFin-OpYNI1-tPEX10	IMX2566	This study
IMX2565	MATa ku70Δ::pTEF1-Spcas9-tTEF12::pGPD-EcdsdAMX4-tLIP2 E_4Δ::pTEFin-OpCNX1-tPEX10 pGPD-OpCNX2-tLIP2 C_2Δ::pTEFin-OpNFS1-tPEX10 pGPD-OpCNX3-tLIP2 E_1Δ::pTEFin-OpCNX3-tPEX10 pGPD-CrMoT1.tLIP2 C_3Δ::pTEFin-OpYNR1-tPEX10 pGPD-OpYNT1.tLIP2 pTEFin-OpYNI1-tPEX10 E_3Δ::pTEFin-OpCNX6-tPEX10 pGPD-OpCNX5-tLIP2	IMX2267	This study
IMS1174	MATa ku70Δ::pTEF1-Spcas9-tTEF12::pGPD-EcdsdAMX4-tLIP2 E_4Δ::pTEFin-OpCNX1-tPEX10 pGPD-OpCNX2-tLIP2 C_2Δ::pTEFin-OpNFS1-tPEX10 pGPD-OpCNX3-tLIP2 E_1Δ::pTEFin-OpCNX3-tPEX10 pGPD-CrMoT1.tLIP2 C_3Δ::pTEFin-OpYNR1-tPEX10 pGPD-OpYNT1.tLIP2 pTEFin-OpYNI1-tPEX10 E_3Δ::pTEFin-OpCNX6-tPEX10 pGPD-OpCNX5-tLIP2 (Evolved on SMD_{NO3} for 21 transfers. Line 2–Colony 1)	IMX2565	This study
IMS1175	MATa ku70Δ::pTEF1-Spcas9-tTEF12::pGPD-EcdsdAMX4-tLIP2 E_4Δ::pTEFin-OpCNX1-tPEX10 pGPD-OpCNX2-tLIP2 C_2Δ::pTEFin-OpNFS1-tPEX10 pGPD-OpCNX3-tLIP2 E_1Δ::pTEFin-OpCNX3-tPEX10 pGPD-CrMoT1.tLIP2 C_3Δ::pTEFin-OpYNR1-tPEX10 pGPD-OpYNT1.tLIP2 pTEFin-OpYNI1-tPEX10 E_3Δ::pTEFin-OpCNX6-tPEX10 pGPD-OpCNX5-tLIP2 (Evolved on SMD_{NO3} for 21 transfers. Line 2–Colony 2)	IMX2565	This study
IMS1176	MATa ku70Δ::pTEF1-Spcas9-tTEF12::pGPD-EcdsdAMX4-tLIP2E_4Δ::pTEFin-OpCNX1-tPEX10 pGPD-OpCNX2-tLIP2 C_2Δ::pTEFin-OpNFS1-tPEX10 pGPD-OpCNX3-tLIP2 E_1Δ::pTEFin-OpCNX3-tPEX10 pGPD-CrMoT1.tLIP2 C_3Δ::pTEFin-OpYNR1-tPEX10 pGPD-OpYNT1.tLIP2 pTEFin-OpYNI1-tPEX10 E_3Δ::pTEFin-OpCNX6-tPEX10 pGPD-OpCNX5-tLIP2 (Evolved on SMD_{NO3} for 21 transfers. Line 2–Colony 3)	IMX2565	This study
IMS1177	MATa ku70Δ::pTEF1-Spcas9-tTEF12::pGPD-EcdsdAMX4-tLIP2 E_4Δ::pTEFin-OpCNX1-tPEX10 pGPD-OpCNX2-tLIP2 C_2Δ::pTEFin-OpNFS1-tPEX10 pGPD-OpCNX3-tLIP2 E_1Δ::pTEFin-OpCNX3-tPEX10 pGPD-CrMoT1.tLIP2 C_3Δ::pTEFin-OpYNR1-tPEX10 pGPD-OpYNT1.tLIP2 pTEFin-OpYNI1-tPEX10 E_3Δ::pTEFin-OpCNX6-tPEX10 pGPD-OpCNX5-tLIP2 (Evolved on SMD_{NO3} for 21 transfers. Line 3–Colony 1)	IMX2565	This study
IMS1178	MATa ku70Δ::pTEF1-Spcas9-tTEF12::pGPD-EcdsdAMX4-tLIP2 E_4Δ::pTEFin-OpCNX1-tPEX10 pGPD-OpCNX2-tLIP2 C_2Δ::pTEFin-OpNFS1-tPEX10 pGPD-OpCNX3-tLIP2 E_1Δ::pTEFin-OpCNX3-tPEX10 pGPD-CrMoT1.tLIP2 C_3Δ::pTEFin-OpYNR1-tPEX10 pGPD-OpYNT1.tLIP2 pTEFin-OpYNI1-tPEX10 E_3Δ::pTEFin-OpCNX6-tPEX10 pGPD-OpCNX5-tLIP2 (Evolved on SMD_{NO3} for 21 transfers. Line 3–Colony 2)	IMX2565	This study

Table 1. Continued

Name	Relevant genotype	Parental strain	Reference
IMS1179	MATa ku70Δ::pTEF1-Spcas9-tTEF12::pGPD-EcdsdAMX4-tLIP2 E.4Δ::pTEFin-OpCNX1-tPEX10 pGPD-OpCNX2-tLIP2 C.2Δ::pTEFin-OpNFS1-tPEX10 pGPD-OpCNX3-tLIP2 E.1Δ::pTEFin-OpCNX3-tPEX10 pGPD-CrMoT1.tLIP2 C.3Δ::pTEFin-OpYNR1-tPEX10 pGPD-OpYNT1.tLIP2 pTEFin-OpYNI1-tPEX10 E.3Δ::pTEFin-OpCNX6-tPEX10 pGPD-OpCNX5-tLIP2 (Evolved on SMD$_{NO3}$ for 21 transfers. Line 3–Colony 3)	IMX2565	This study
IMS1180	MATa ku70Δ::pTEF1-Spcas9-tTEF12::pGPD-EcdsdAMX4-tLIP2 E.4Δ::pTEFin-OpCNX1-tPEX10 pGPD-OpCNX2-tLIP2 C.2Δ::pTEFin-OpNFS1-tPEX10 pGPD-OpCNX3-tLIP2 E.1Δ::pTEFin-OpCNX3-tPEX10 pGPD-CrMoT1.tLIP2 C.3Δ::pTEFin-OpYNR1-tPEX10 pGPD-OpYNT1.tLIP2 pTEFin-OpYNI1-tPEX10 E.3Δ::pTEFin-OpCNX6-tPEX10 pGPD-OpCNX5-tLIP2 (Evolved on SMD$_{NO3}$ for 21 transfers. Line 1–Colony 1)	IMX2565	This study
IMS1181	MATa ku70Δ::pTEF1-Spcas9-tTEF12::pGPD-EcdsdAMX4-tLIP2 E.4Δ::pTEFin-OpCNX1-tPEX10 pGPD-OpCNX2-tLIP2 C.2Δ::pTEFin-OpNFS1-tPEX10 pGPD-OpCNX3-tLIP2 E.1Δ::pTEFin-OpCNX3-tPEX10 pGPD-CrMoT1.tLIP2 C.3Δ::pTEFin-OpYNR1-tPEX10 pGPD-OpYNT1.tLIP2 pTEFin-OpYNI1-tPEX10 E.3Δ::pTEFin-OpCNX6-tPEX10 pGPD-OpCNX5-tLIP2 (Evolved on SMD$_{NO3}$ for 21 transfers. Line 1–Colony 2)	IMX2565	This study
IMS1182	MATa ku70Δ::pTEF1-Spcas9-tTEF12::pGPD-EcdsdAMX4-tLIP2 E.4Δ::pTEFin-OpCNX1-tPEX10 pGPD-OpCNX2-tLIP2 C.2Δ::pTEFin-OpNFS1-tPEX10 pGPD-OpCNX3-tLIP2 E.1Δ::pTEFin-OpCNX3-tPEX10 pGPD-CrMoT1.tLIP2 C.3Δ::pTEFin-OpYNR1-tPEX10 pGPD-OpYNT1.tLIP2 pTEFin-OpYNI1-tPEX10 E.3Δ::pTEFin-OpCNX6-tPEX10 pGPD-OpCNX5-tLIP2 (Evolved on SMD$_{NO3}$ for 21 transfers. Line 1–Colony 3)	IMX2565	This study
IMS1183	MATa ku70Δ::pTEF1-Spcas9-tTEF12::pGPD-EcdsdAMX4-tLIP2 E.4Δ::pTEFin-OpCNX1-tPEX10 pGPD-OpCNX2-tLIP2 C.2Δ::pTEFin-OpNFS1-tPEX10 pGPD-OpCNX3-tLIP2 E.1Δ::pTEFin-OpCNX3-tPEX10 pGPD-CrMoT1.tLIP2 C.3Δ::pTEFin-OpYNR1-tPEX10 pGPD-OpYNT1.tLIP2 pTEFin-OpYNI1-tPEX10 E.3Δ::pTEFin-OpCNX6-tPEX10 pGPD-OpCNX5-tLIP2 (Evolved on SMD$_{NO3}$ for 50 transfers. Evolved population line 2)	IMX2565	This study
IMS1184	MATa ku70Δ::pTEF1-Spcas9-tTEF12::pGPD-EcdsdAMX4-tLIP2 E.4Δ::pTEFin-OpCNX1-tPEX10 pGPD-OpCNX2-tLIP2 C.2Δ::pTEFin-OpNFS1-tPEX10 pGPD-OpCNX3-tLIP2 E.1Δ::pTEFin-OpCNX3-tPEX10 pGPD-CrMoT1.tLIP2 C.3Δ::pTEFin-OpYNR1-tPEX10 pGPD-OpYNT1.tLIP2 pTEFin-OpYNI1-tPEX10 E.3Δ::pTEFin-OpCNX6-tPEX10 pGPD-OpCNX5-tLIP (Evolved on SMD$_{NO3}$ for 50 transfers. Evolved population line 3)	IMX2565	This study
IMS1185	MATa ku70Δ::pTEF1-Spcas9-tTEF12::pGPD-EcdsdAMX4-tLIP2 E.4Δ::pTEFin-OpCNX1-tPEX10 pGPD-OpCNX2-tLIP2 C.2Δ::pTEFin-OpNFS1-tPEX10 pGPD-OpCNX3-tLIP2 E.1Δ::pTEFin-OpCNX3-tPEX10 pGPD-CrMoT1.tLIP2 C.3Δ::pTEFin-OpYNR1-tPEX10 pGPD-OpYNT1.tLIP2 pTEFin-OpYNI1-tPEX10 E.3Δ::pTEFin-OpCNX6-tPEX10 pGPD-OpCNX5-tLIP2 (Evolved on SMD$_{NO3}$ for 50 transfers. Evolved population line 1)	IMX2565	This study

Bacto tryptone, 5 g/L Bacto yeast extract and 5 g/L NaCl) supplemented with 100 mg/L ampicillin. *Yarrowia lipolytica* and *E. coli* cultures were stored at −80°C after the addition of 30% v/v glycerol.

Molecular biology techniques

Primers used in this study are shown in Table 2. DNA was amplified using either Phusion Hot Start II High Fidelity Polymerase (Thermo Fisher Scientific, Waltham, MA) or Phusion U (Thermo Fisher Scientific) and desalted or PAGE-purified oligonucleotide primers (Sigma-Aldrich, St-Louis, MO) according to manufacturers' instructions. Diagnostic PCR reactions were performed with DreamTaq polymerase (Thermo Fisher Scientific). PCR products were separated by gel electrophoresis on a 1% (w/v) agarose gel (Thermo Scientific) in TAE buffer (40 mM Tris, 20 mM acetic acid and 1 mM EDTA; Thermo Scientific) and purified with a Zymoclean Gel DNA Recovery Kit (Zymo Research, Irvine, CA). Plasmids were isolated from *E. coli* using a NucleoSpin Plasmid kit (Macherey-Nagel, Düren, Germany), and verified by either restriction digestion or diagnostic PCR. *Escherichia coli* DH5-*α* (New England BioLabs, Ipswich, MA) was used for cloning procedures (Inoue, Nojima and Okayama 1990). Yeast genomic DNA used for diagnostic PCR reactions was isolated by using the SDS/LiAc protocol (Looke, Kristjuhan and Kristjuhan 2011). *Yarrowia lipolytica* transformation was performed with the LiAc method as previously described (Chen, Beckerich and Gaillardin 1997). A total of four to eight colonies were re-streaked on selective medium to select for single clones and diagnostic PCRs were performed to verify the correct genotypes.

Plasmid construction

Plasmids used in this study are shown in Table 3. Gene sequences coding for proteins involved in Moco biosynthesis (*OpCNX1*, *OpCNX2, OpCNX3*, *OpCNX4*, *OpCNX5*, *OpCNX6* and *OpNFS1*) nitrate assimilation (*OpYNT1*, *OpYNR1* and *OpYNI1*) were retrieved from *O. parapolymorpha* DL-1 genome sequence (Ravin *et al.* 2013; Perli *et al.* 2021) BioProject PRJNA60503. A gene coding for a previously characterized high-affinity molybdenum transporter, *CrMoT1,* from *C. reinhardtii* was also included in the gene-set (Tejada-Jimenez *et al.* 2007). Each gene was codon-optimized for expression in *Y. lipolytica* using the GeneOptimizer tool (Thermo Fisher Scientific) and ordered as synthetic DNA from GeneArt (Thermo Fisher Scientific) resulting in plasmids pUD1057 (*OpCNX6*), pUD1058 (*OpCNX4*), pUD1059 (*OpCNX5*), pUD1060 (*OpNFS1*), pUD1061 (*OpCNX1*), pUD1062 (*OpCNX2*), pUD1063 (*CrMoT1*) pUD1064 (*OpCNX4*), pUD1065 (*OpYNR1*), pUD1066 (*OpYNI1*) and pUD1067 (*OpYNT1*). Single-gene Biobricks compatible with USER cloning (New England BioLabs) were amplified from pUD1057, pUD1058, pUD1059, pUD1060, pUD1061, pUD1062, pUD1063, pUD1064, pUD1065, pUD1066 and pUD1067 using primer pairs 24487/24488, 24485/24486, 24489/24490, 24483/24484, 24479/24480, 24481/24482, 24491/24492, 24493/24494, 24495/24496, 24499/24500 and 24497/24498, respectively. Single promoter Biobricks pTEFin and pGPD were amplified from ST6512 genomic DNA using primer pairs 22956/24013 and 15529/15528, respectively. Then, a Biobrick carrying the back-to-back promoter pair pTEFin-pGPD was cloned by USER cloning (Bitinaite *et al.* 2007) fusion of the two single-promoter Biobricks and primer pair 22956/15528. A single promoter pTEFin Biobrick was amplified using ST6512 genomic DNA and primer pair 27208/22956.

Backbone Biobricks for the integration at the E_4, C_2, E_1, E_3, C_3 and D_1 integration sites were prepared by digestion and nicking of plasmids pCfB6679, pCfB6682, pCfB6677, pCfB6681, pCfB6371 and pCfB6684, respectively, using endonuclease FastDigest AsiSI (Life Technologies, Carlsbad, CA) and Nb.BsmI (New England BioLabs) followed by gel purification as previously described (Holkenbrink *et al.* 2018). A backbone E_4 Biobrick was combined with Biobricks pTEFin-pGPD, *OpCNX1* and *OpCNX2* in a USER cloning reactions as previously described (Holkenbrink *et al.* 2018) to yield plasmid CfB8966. Similarly, plasmids pCfB8967, pCfB8968, pCfB8969, and pCfB8970 were cloned by combining a pTEFin-pGPD promoter Biobrick with a C_2, E_1, E_3 or C_3 backbone, respectively, and gene Biobricks *OpNFS1/OPCNX4*, *OpCNX6/OpCNX5*, *CrMOT1/OpCNX3* and *OpYNR1/OpYNT1*, respectively. Plasmid pCfB8971 was cloned by combining a D_1 backbone Biobrick with a pTEFin promoter and *OpYNI1* gene Biobricks. Gibson assembly (Gibson *et al.* 2009) was used to construct the integration plasmid pCfB9006 that carries overexpression cassettes for *OpCNX3*, *CrMoT1*, *OpCNX5* and *OpCNX6*. First, the plasmid pCfB8968 carrying the *OpCNX5-OpCNX6* cassette was linearized with primers 24522/24517 and the *OpCNX3-CrMoT1* cassette was amplified using primers 24518/24523 and pCfB8969 as template. Secondly, the GFPmut3 spacer cassette (Andersen *et al.* 1998) was amplified from plasmid pI774 with primer pairs 24520/24521. Each fragment was gel-purified and combined in equimolar amounts in a Gibson reaction following manufacturer's instructions to form pCfB9006. In a similar way, the integration plasmid pCfB9007, carrying nitrate assimilation pathway was cloned by combining a *OpYNT1-OpYNR1* cassette with an *OpYNI1* cassette and a GFPmut3 spacer. Plasmid pCfB8970 was linearized with primers 24524/24517 while the *OpYNI1* cassette was amplified with primers 24525/24518 and pCfB8971 as template. Plasmid pUDI264 for the integration of *OpCNX5-OpCNX6* at the E_3 integration site was cloned by Gibson assembly by combining a backbone fragment amplified with primers 17889/17890 and pCfB6681 as template and a fragment carrying the *OpCNX5-OpCNX6* cassette amplified with primers 17887/17888 and pCfB8968 as template. Correct plasmid assembly was verified by Sanger sequencing.

Strain construction

CRISPR/Cas9-mediated marker-free gene integration in *Y. lipolytica* was performed following the EASYcloneYali method as previously described (Holkenbrink *et al.* 2018). In brief, 1 μg of NotI (Thermo Fisher Scientific) digested integrative plasmid carrying two or more genes flanked by long-homology arms to the integration *locus* was co-transformed together with 500 ng of a plasmid for the expression of a gRNA targeting the *locus* of interest. After selection and correct genotyping of transformants via diagnostic PCR, one colony of correct clone was inoculated in a 50-mL Greiner tube containing 20 ml YPD and incubated overnight at 30°C, 200 rpm to allow the gRNA plasmid loss. The next day, cells were streaked to single colonies on a YPD plate and then, after incubation at 30°C overnight, single colonies were patched on both selective and non-selective media. One plasmid-free colony was then picked and grown overnight in a YPD flask prior stocking at −80°C.

First, strain ST6512 was transformed with NotI-digested pCfB8966 and the E_4 targeting gRNA expression plasmid pCfB6638 to yield IMX2264. Then, IMX2264 was transformed with NotI-digested pCfB8967 and the C_2 targeting gRNA expression plasmid pCfB6682 to yield IMX2265. IMX2266 was obtained

Table 2. Primers used in this study.

Primer number	Primer sequence	Product(s)
22956	AGTACTGCAAAAAGUGCTGGTCGG	PrTEFin-PrGPD_USER.Biobrick
24013	ATCAGTAGCUAGAGACCGGGTTGGCGGCG	PrTEFin-PrGPD_USER.Biobrick
15529	AGCTACTGAUGAGCGAGTAGGATGTCCTGCACGG	PrTEFin-PrGPD_USER.Biobrick
15528	ATGACAGAUTGTTGAtGTGTGTTTAATTCAAGAATG	PrTEFin-PrGPD_USER.Biobrick
27208	ACACGCGAUAGAGACCGCGGTTGGCGG	PrTEFin_USER.Biobrick
22956	AGTACTGCAAAAAGUGCTGGTCGG	PrTEFin_USER.Biobrick
24479	ACTTTTTGCAGTACUAACCGCAGCCCGTGCGACACCTG	OpCNX1_USER.Biobrick
24480	CGTGCGAUTTAGCCGCCGATCAGG	OpCNX1_USER.Biobrick
24481	ATCTGTCAUGCCACAATGGTGGCCATCCACG	OpCNX2_USER.Biobrick
24482	CACGCGAUTTACTTGAAGATGTAGACAGGTCG	OpCNX2_USER.Biobrick
24483	ACTTTTTGCAGTACUAAACCGAGTACCGATTCCGAATTGGAGC	OpNFS1_USER.Biobrick
24484	CGTGCGAUTTAGTGTCCGGCCCACTC	OpNFS1_USER.Biobrick
24485	ATCTGTCAUGCCACAATGTCTCTGTCTCTGAACGAGTAC	OpCNX4_USER.Biobrick
24486	CACGCGAUTTAGTAGATGGGGAAGTTAGGGTC	OpCNX4_USER.Biobrick
24487	ACTTTTTGCAGTACUAAACCGAGTCTATCTTCGTGGACATCACC	OpCNX6_USER.Biobrick
24488	CGTGCGAUTTAGGTTCGAGACAGCACG	OpCNX6_USER.Biobrick
24489	ATCTGTCAUGCCACAATGGTGGCCGTGGC	OpCNX5_USER.Biobrick
24490	CACGCGAUTTAGCCAGAGGACACAGGAG	OpCNX5_USER.Biobrick
24491	ACTTTTTGCAGTACUAAACCGCGAGGCCCTGCAGAACGCC	CrMoT1_USER.Biobrick
24492	CGTGCGAUTTAGGCTCGGCCGC	CrMoT1_USER.Biobrick
24493	ATCTGTCAUGCCACAATGACCGTGGGCATCC	OpCNX3_USER.Biobrick
24494	CACGCGAUTTACACGTAGATCTCGTCGATC	OpCNX3_USER.Biobrick
24495	ACTTTTTGCAGTACUAAACCGCGAGGACTCTGTGGTGACCGAGGT	OpYNR1_USER.Biobrick
24496	CGTGCGAUTTAGAAGTAGACCACGTACTGCTTGTC	OpYNR1_USER.Biobrick
24497	ATCTGTCAUGCCACAATGGGACTGCTCTACCCTGTG	OpYNT1_USER.Biobrick
24498	CACGCGAUTTAGATCTCGGCCTTTCGG	OpYNT1_USER.Biobrick
24499	ACTTTTTGCAGTACUAAACCGCAGACCTGCTCTGTGCCTC	OpYNI1_USER.Biobrick
24500	CGTGCGAUTTACCAGTCGAAAGAGATGGC	OpYNI1_USER.Biobrick
24517	TAGATAAATTTACACTCCCTCAGATGCATTCTTGGGCGGT	pCfB9006-7.backbone.Gibson.fragment
24518	TCATGGGCCTTCCTTTCACTCAGATGCATTCTTGGGCGGT	pCfB9006-7.2-genes.insert.Gibson.fragment
24520	ACCGCCCAAGAAATGCCATCTGAGGGAGTGTAAATTTATCTATACAGAGGTAA	pI774.GFPmut3b.spacer.Gibson.fragment
24521	ACCGCCCAAGAAATGCCATCTGAGTGAAAGGAAGGCCCATGA	pI774.GFPmut3b.spacer.Gibson.fragment
24522	TTCATTCATGTTAGTTGCGTTCTGCGTCTGTTTGTGTC	pCfB9006.backbone.Gibson.fragment
24523	ACACAAACAGCAGACGCGAGAAGCCAACTAACATGAATGAATACGATATACA	pCfB9006.2-genes.insert.Gibson.fragment
24524	TTCATTCATGTTAGTTGCGTGCCATAGCACTATTGTAGAGTGGCC	pCfB9007.backbone.Gibson.fragment
24525	CTCTACAATAGTGCTATGGCACGCAACTAACATGAATGAATACGATATACA	pCfB9007.2-genes.insert.Gibson.fragment
17887	TCACTTCCCCATCCACACTTTTAGGTTCGAGACAGCACGT	pUDI264.insert.Gibson.fragment
17888	AGGTTGATTCCGAACAGAAGTTAGCCAGAGGACACAGGAG	pUDI264.insert.Gibson.fragment
17889	CTCCTGTGTCCTCTGGCTAACTTCTGTTCGGAATCAACCTC	pUDI264.backbone.Gibson.fragment
17890	ACGTGCTGCTCTCGAACCTAAAAGTGTGATGGGGAAGTGA	pUDI264.backbone.Gibson.fragment

Table 3. Plasmids used in this study.

Name	Characteristics	Reference
pCfB6371	*bla* ColE1 ^{NotI}C_3–3′homology *tPEX20-tLIP2* C_3–5′homology^{NotI}	Holkenbrink *et al.* (2018)
pCfB6677	*bla* ColE1 ^{NotI}E_1–3′homology *tPEX20-tLIP2* E_1–5′homology^{NotI}	Holkenbrink *et al.* (2018)
pCfB6679	*bla* ColE1 ^{NotI}E_4–3′homology *tPEX20-tLIP2* E_4–5′homology^{NotI}	Holkenbrink *et al.* (2018)
pCfB6681	*bla* ColE1 ^{NotI}E_3–3′homology *tPEX20-tLIP2* E_3–5′homology^{NotI}	Holkenbrink *et al.* (2018)
pCfB6682	*bla* ColE1 ^{NotI}C_2–3′homology *tPEX20-tLIP2* C_2–5′homology^{NotI}	Holkenbrink *et al.* (2018)
pCfB6684	*bla* ColE1 ^{NotI}D_1–3′homology *tPEX20-tLIP2* D_1–5′homology^{NotI}	Holkenbrink *et al.* (2018)
pCfB6627	*bla* ColE1 NAT gRNA_C_2	Holkenbrink *et al.* (2018)
pCfB6630	*bla* ColE1 NAT gRNA_C_3	Holkenbrink *et al.* (2018)
pCfB6631	*bla* ColE1 NAT gRNA_D_1	Holkenbrink *et al.* (2018)
pCfB6633	*bla* ColE1 NAT gRNA_E_1	Holkenbrink *et al.* (2018)
pCfB6637	*bla* ColE1 NAT gRNA_E_3	Holkenbrink *et al.* (2018)
pCfB6638	*bla* ColE1 NAT gRNA_E_4	Holkenbrink *et al.* (2018)
pI774	*bla* ColE1 *Gfpmut3*	Unpublished
pUD1057	*bla* ColE1 *OpCNX6**	GeneArt
pUD1058	*bla* ColE1 *OpCNX4**	GeneArt
pUD1059	*bla* ColE1 *OpCNX5**	GeneArt
pUD1060	*bla* ColE1 *OpNFS1**	GeneArt
pUD1061	*bla* ColE1 *OpCNX1**	GeneArt
pUD1062	*bla* ColE1 *OpCNX2**	GeneArt
pUD1063	*bla* ColE1 *CrMoT1**	GeneArt
pUD1064	*bla* ColE1 OpCNX3*	GeneArt
pUD1065	*bla* ColE1 *OpYNR1**	GeneArt
pUD1066	*bla* ColE1 *OpYNI1**	GeneArt
pUD1067	*bla* ColE1 *OpYNT1**	GeneArt
pCfB8966	*bla* ColE1 ^{NotI}E_4–3′homology *tPEX20-OpCNX1*-pTEF1in-pGPD-OpCNX2*-tLIP2* E_4–5′homology^{NotI}	This study
pCfB8967	*bla* ColE1 ^{NotI}C_2–3′homology *tPEX20-OpNFS1*-pTEF1in-pGPD-OpCNX4*-tLIP2* C_2–5′homology^{NotI}	This study
pCfB8968	*bla* ColE1 ^{NotI}E_1–3′homology *tPEX20-OpCNX6*-pTEF1in-pGPD-OpCNX5*-tLIP2* E_1–5′homology^{NotI}	This study
pCfB8969	*bla* ColE1 ^{NotI}E_3–3′homology *tPEX20-CrMoT1*-pTEF1in-pGPD-OpCNX3*-tLIP2* E_3–5′homology^{NotI}	This study
pCfB8970	*bla* ColE1 ^{NotI}C_3–3′homology *tPEX20-OpYNR1*-pTEF1in-pGPD-OpYNT1*-tLIP2* C_3–5′homology^{NotI}	This study
pCfB8971	*bla* ColE1 ^{NotI}D_1–3′homology *tPEX20-OpYNI1*-pTEF1in- tLIP2* D_1–5′homology^{NotI}	This study
pCfB9006	*bla* ColE1 ^{NotI}E_1–3′homology *tPEX20-OpCNX6*-pTEF1in-pGPD-OpCNX5*-tLIP2 Gfpmut3 tPEX20-CrMoT1*-pTEF1in-pGPD-OpCNX3*-tLIP2* E_1–5′homology^{NotI}	This study
pCfB9007	*bla* ColE1 ^{NotI}C_3–3′homology *tPEX20-OpYNR1*-pTEF1in-pGPD-OpYNT1*-tLIP2 Gfpmut3 tPEX20-OpYNI1*-pTEF1in- tLIP2* C_3–5′homology^{NotI}	This study
pUDI264	*bla* ColE1 ^{NotI}E_3–3′homology *tPEX20-OpCNX6*-pTEF1in-pGPD-OpCNX5*-tLIP2* E_3–5′homology^{NotI}	This study

*Codon optimized for expression in *Y. lipolytica*.

by transforming IMX2265 with NotI-digested pCfB9006 and the E_1 targeting gRNA expression plasmid pCfB6633. IMX2264 was transformed with NotI-digested pCfB9007 and the C_3 targeting gRNA expression plasmid pCfB6630 to yield IMX2267. Whole genome re-sequencing of IMX2267 revealed that *OpCNX5* and *OpCNX5* were not integrated but instead *CrMoT1* and *OpCNX3* were present in two copies (PRJNA704845). To correct this absence, IMX2267 was subsequently transformed with NotI-digested pUDI264 together with the E_3 targeting gRNA expression plasmid pCfB6637, to yield the final strain IMX2565. The presence of all integrated genes in IMX2565 was confirmed by whole genome re-sequencing (PRJNA704845).

ALE

To evolve IMX2565 for fast growth in nitrate-containing media, the strain was inoculated in triplicate in 100-mL flasks containing 20 ml SMD$_{NO3}$. Flasks were incubated at 30°C, 200 rpm until OD$_{660}$ reached a value above 5. Then, 0.2 mL of each cul-

ture was transferred in a new shake flask containing the same medium and incubated again. This process was repeated for 50 times, corresponding to approximately 335 generations, after which the evolved population were stocked and named IMS1183 (line 1), IMS1184 (line 2) and IMS1185 (line 3). Glycerol stocks for each evolution line were also prepared at intermediate steps after 3, 6, 9, 12, 21, 27, 38 and 50 transfers. Before transferring the cultures from batch 21, single colonies were isolated by restreaking each culture on SMD$_{NO3}$ agar plates. After incubation of the plates at 30°C in a static incubator for 48 h, three single colonies for each evolution line were picked and inoculated in 100-mL shake flasks containing 20 mL SMD$_{NO3}$. Flasks were incubated for 48 h at 30°C, 200 rpm and the grown biomass was then stocked at −80°C by the addition of 30% v/v glycerol and named IMS1174 (line 2, colony 1), IMS1175 (line 2, colony2), IMS1176 (line 2, colony 3), IMS1177 (line 3, colony 1), IMS1178 (line 3, colony 2), IMS1179 (line 3, colony 3), IMS1180 (line 1, colony 1), IMS1181 (line 1, colony 2) and IMS1182 (line 1, colony 3).

High-throughput strain cultivation and growth rate estimation

The growth rate of strains IMS1174, IMS1175, IMS1176, IMS1177, IMS1178, IMS1179, IMS1180, IMS1181 and IMS1182, together with the three evolved populations IMX1183, IMS1184 and IMS1185 at batch number 3, 6, 9, 15, 21, 38 and 50, were estimated by cultivation in 96 deep-well plates in a Growth Profiler 960 instrument (Enzyscreen, Heemstede, The Netherlands). A glycerol stock for each strain was inoculated in a 100-mL shake flask containing 20 mL SMD_{NO3} and incubated overnight at 30°C, 200 rpm. The next day, each culture was centrifuged at 3000 g for 5 min, supernatant was discarded and cell pellets were resuspended in SMD_{NO3} to and OD_{660} of 5. Then, two 96 deep-well plates were filled with 250 µL of SMD_{NO3} medium and each well was inoculated with 5 µL of one of the tested strains. Each strain was inoculated in triplicate with the exception of IMS1174, IMS1176, IMS1178, IMS1179, IMS1181 and IMS1182 that were inoculated in duplicate. Plates were incubated at 30°C, 250 rpm until the cultures reached stationary phase. To convert the measured 'green' cell density values into OD_{660} equivalent, a calibration curve was prepared by correlating the 'green' value of a IMS2565 cultures in SMD_{Urea} at eight different OD_{660} values that were measured externally with a 7200 Jenway Spectrophotometer (Jenway, Stone, UK). Moreover, values measured for each position in the plate were normalized by a factor that was calculated by measuring the green value of a IMS2565 culture in SMD_{Urea} of $OD_{660} = 5$ and by dividing that value by the average value measured across the whole plate (position normalization). After normalizing each green value time point by its own position normalization factor, OD_{660} equivalent values were calculated by fitting values with the calibration curve. Growth rate of each culture was calculated by fitting the exponential growth function with points of OD_{660} equivalent values between 0.5 and 2.

Aerobic cultivation in shake flasks

For the determination of the growth rate of IMS1174, IMS1175, IMS1176, IMS1177, IMS1178, IMS1179, IMS1180, IMS1181, IMS1182, IMX1183, IMS1184 and IMS1185, frozen stock cultures were used to inoculate 20 mL SMD_{NO3} starter cultures. These were subsequently used to inoculate 100 mL SMD_{NO3} flask cultures to initial OD_{660} values between 0.1 and 0.2. Growth of these cultures was monitored with a 7200 Jenway Spectrophotometer (Jenway). Specific growth rates were calculated from at least five time points in the exponential growth phase of each culture. At each time point, 2 mL of liquid culture was centrifuged for 5 min at 14 000 g, and supernatant was collected for HPLC and nitrate, nitrite, and ammonia analysis.

Whole-genome sequencing

Genomic DNA of strains ST6512, IMX2267, IMX2565, IMS1175, IMS1177 and IMS1180 was isolated with a Blood and Cell Culture DNA Kit with 100/G Genomics-tips (QIAGEN, Hilden, Germany) following manufacturer's instructions. Illumina-based paired-end sequencing with 150-bp reads was performed on 550-bp TruSeq DNA PCR-free insert libraries with a minimum resulting coverage of 50 x (Macrogen-Europe, Amsterdam, The Netherlands). Data mapping was performed using bwa 0.7.15-r1142-dirty against the *Y. lipolytica* CLIB122 genome (Kerscher *et al.* 2001; Dujon *et al.* 2004) to which five extra contigs containing the relevant integration cassettes had been previously added.

Data processing and chromosome copy number variation determinations were done as previously described (Nijkamp *et al.* 2012; Perli *et al.* 2020) except for VCF file intersection and annotation that was performed with VCFtools 0.1.13 (vcf-isec command) and SnpEff, respectively (Danecek *et al.* 2011; Cingolani *et al.* 2012).

In vitro nitrate reductase activity measurements from cell extract

Nitrate reductase activity was measured from cell extract of strain ST6512, IMX2565, IMS1175, IMS1177, IMS1180 and IMX2565 evolution lines 1, 2 and 3. Cell extract preparation and activity measurements were performed as previously described (Perli *et al.* 2021). In brief, frozen stock cultures of each tested strain and evolved populations were used to inoculate 20 mL starter cultures, which were then used to inoculate 100 mL shake flask cultures on the same medium, to an initial OD_{660} of 0.2. Shake flasks were incubated until the OD_{660} exceeded 40. All strains were grown on SMD_{urea} with the exception of the evolution lines 1, 2 and 3 that were grown on SMD_{NO3}. Cultures were then centrifuged at 3000 g for 5 min, supernatant was discarded and cell pellets were resuspended in 2 mL lysis buffer (100 mM KPO_4 pH 7 supplemented with complete ULTRA EDTA-free protease inhibitor cocktail, Roche, Basel, Switzerland). Cell resuspensions were aliquoted in 1.5 mL bead-beating tubes along with 0.75 g of 400–600 µm acid-washed glass beads (Sigma Aldrich) per tube. Cells were disrupted by six 1-min cycles at 5 m/s speed in a Fast-Prep 24 cell homogenizer (MP Biomedicals, Santa Ana, CA), with 5-min cooling on ice between cycles. Glass beads were separated from the cell extract by centrifuging the tubes for 10 min at 4°C and 15 000 g on a tabletop centrifuge. Supernatant was recovered in a fresh tube and clarified by centrifuging for 1 h at 4°C, 20 000 rpm. Clarified cell extracts were recovered and diluted 10 times in lysis buffer and kept on ice prior to analysis. Nitrate reductase activity was measured by monitoring substrate dependent NADPH consumption at 340 nm using a spectrophotometer (Jasco, Easton, MA). Reactions were performed in 1 mL final volume of 100 mM KPO_4 buffer pH 7 supplemented with 200 µM NADPH, 20 µM FAD, 1 mM KNO_3 as substrate and either 50 or 25 µL of clarified cell extract. Protein contents of cell extracts were quantified with a Quick Start Bradford Assay (Bio-Rad Laboratories, Hercules, CA) following manufacturer's instructions. Specific activities of nitrate reductase in cell extracts were expressed in μmol $NADP^+$ min^{-1} $mg_{protein}^{-1}$.

In silico mitochondrial targeting prediction

The likelihood of mitochondrial targeting for the wild-type and mutated *Op*Cnx1 and *Op*Cnx2 sequences were calculated using five different web-based tools: TargetP 2.0 (Almagro Armenteros *et al.* 2019), DeepLoc 1.0 (Almagro Armenteros *et al.* 2017), Mito-Fates (Fukasawa *et al.* 2015), Predotar (Small *et al.* 2004) and PredSL (Petsalaki *et al.* 2006). When possible, non-plant or fungal database was selected as option.

Analytical methods

Metabolite concentrations in culture supernatants were analysed by high-performance liquid chromatography (HPLC) on an Agilent 1260 HPLC (Agilent Technologies, Santa Clara, CA) fitted with a Bio-Rad HPX 87 H column (Bio-Rad). The flow rate was set at 0.6 mL/min, 0.5 g/L H_2SO_4 was used as eluent and the column

temperature was set at 65°C. An Agilent refractive-index detector and an Agilent 1260 VWD detector were used for metabolite quantification (Verhoeven *et al.* 2017). Nitrate, nitrite and ammonium concentrations in culture supernatants were measured with a Hach DR3900 spectrophotometer and Hach kits LCK 339, LCK 341 and LCK 304 (Hach Lange, Düsseldorf, Germany), according to the manufacturer's instructions.

Statistical analysis

Statistical significance of differences between measurements from replicate samples were calculated by using a two-tailed t-test assuming unequal variances (Welch's correction).

Data availability

All measurement data and calculations used for each figure in the manuscript are available at the 4TU.Centre for research data repository (https://researchdata.4tu.nl/) under URL:https://doi.org/10.4121/14230238.v1. DNA sequencing data of *Y. lipolytica* strains ST6512, IMX2267, IMX2565, IMS1175, IMS11777 and IMS1180 were deposited at NCBI (https://www.ncbi.nlm.nih.gov/) under BioProject accession number PRJNA704845.

RESULTS

Design and engineering of Moco biosynthesis and nitrate assimilation in *Y. lipolytica*

The absence of molybdenum-dependent enzymes in *Yarrowia* metabolism strongly suggested that the engineering of Moco biosynthesis may not only require functional expression of Moco biosynthesis genes, but also of a high-affinity molybdate transporter (Fig. 1). Based on a previous work in *S. cerevisiae* (Perli *et al.* 2021), it is not fewer than 11 genes from the yeast *O. parapolymorpha* and the algae *C. reinhardtii* that would be required to introduce Moco biosynthesis and nitrate assimilation in *Y. lipolytica*. The gene-set comprises seven genes coding for Moco biosynthesis proteins (*OpCNX1*, *OpCNX2*, *OpCNX3*, *OpCNX4*, *OpCNX5*, *OpCNX6* and *OpNFS1*), three genes coding for the nitrate assimilation pathway (*OpYNT1*, *OpYNR1* and *OpYNI1*) from *O. parapolymorpha*, and one gene coding for the high-affinity molybdate transporter (*CrMoT1*) from *C. reinhardtii* (Fig. 1). The codon-optimized genes were integrated in the chromosome of the *Yarrowia* strain ST6512 (W29, *ku70Δ::pTEF1-Cas9-tTEF12::pGPD-DsdA-tLIP2*) by using CRISPR/Cas9 gene-editing and the EASY-cloneYali promoter parts and integrative plasmids (Holkenbrink *et al.* 2018). Genes were sequentially integrated in five different integration sites (E_4, C_2, E_1, C_3 and E_3) that were previously tested for heterologous gene expression (Holkenbrink *et al.* 2018). At each transformation, two genes were integrated, with the exception of the second last transformation in which all three genes encoding for nitrate assimilation pathway were integrated in one step. After five consecutive transformation rounds, the successful construction of the final strain IMX2565 was confirmed by Illumina short-read sequencing (PRJNA704845; Fig. 2).

ALE on nitrate containing media

Similarly to what was observed in *S. cerevisiae*, adaptation was required to observe growth of the *Y. lipolytica* strain IMX2565 on nitrate medium (Perli *et al.* 2021). We inoculated strain IMX2565 in SMD_{NO3} and incubated the flasks at 30°C in triplicate. Reproducibly, after 2 weeks the *Yarrowia* strain showed full growth (OD_{660} above 20) in all flasks. To improve the strain growth rate, IMX2565 was subjected to ALE by sequential transfers in flasks containing SMD_{NO3} for 335 generations (50 consecutive batches). Evolving cultures were periodically stocked and used to monitor the growth rate of the evolving populations (Fig. 3A). At the onset of the ALE experiment, the initial batches exhibited growth rates ranged from 0.04 to 0.05 h^{-1}. Throughout the first 21st transfers the specific growth rate of the yeast populations increased and levelled off to 0.11–0.12 h^{-1}. At that time-point, corresponding to a about 140 generations, three single colonies were isolated from each evolving culture and named IMS1180 (line 1, colony 1), IMS1181 (line 1, colony 2), IMS1182 (line 1, colony 3), IMS1174 (line 2, colony 1), IMS1175 (line 2, colony2), IMS1176 (line 2, colony 3), IMS1177 (line 3, colony 1), IMS1178 (line 3, colony 2) and IMS1179 (line 3, colony 3). The specific growth rates of the single colony isolates on SMD_{NO3} ranged from 0.03 to 0.09 h^{-1} (Fig. 3B). Clones IMS1180, IMS1175 and IMS1177 were empirically selected for further characterization based on the similar growth performance to the relative evolved populations. The evolution experiment was prolonged for 29 additional sequential batches, summing up to a total of 50 batches (335 generations) to further probe evolvability of the phenotype. However, the growth rate of evolving populations stabilized to a value of about 0.13 h^{-1} and did not further increase (Fig. 3A).

Whole-genome sequencing of evolved strains and mutations identification

To identify mutations responsible for the increase in growth rate, the genomes of clones derived from each evolution line (IMS1175, IMS1177 and IMS1180) and well as those of parental strains (ST6512 and IMX2565) were re-sequenced by Illumina short-read technology. After aligning the reads to the *Y. lipolytica* W29 reference genome (PRJNA601425; Kerscher *et al.* 2001; Dujon *et al.* 2004), mapped data were analysed for the presence of either copy number variations (CNVs), single nucleotide variations (SNVs) and/or insertions/deletions (INDELs) that occurred in the annotated coding sequences. As opposed to what happened in *S. cerevisiae* (Perli *et al.* 2021), no gene or chromosome CNVs were observed between the parental strain IMX2565 and evolved isolates IMS1175, IMS1177 and IMS1180. SNV and INDELs analysis was systematically performed and data from the three sequenced colony isolates were then compared. To minimize the number of miscalls caused by mapping artefacts, SNV and INDELs that were also detected in the two sequenced parental strains ST6512 and IMX2565, mapped to the same reference sequence, were systematically removed. After curation of SNVs and INDELs miscalls, a total of five, two and four mutations were found in evolved isolates IMS1175, IMS1177 and IMS1180, respectively (Fig. 3C and Table 4). While no genes were found mutated in all three independently evolved isolates, three genes (*Spcas9*, *OpCNX1* and YALI0_E24167g) were found differently mutated in two sequenced isolates. The mutations identified in *OpCNX1* that were found in IMS1175 and IMS1177, were identical and located in the 5′ end of the coding sequence (G22A). Since the evolution lines were started independently and the mutation was not present in the engineered strain IMX2565, the recurrence of this mutation in OpCNX1 might be critical in the acquisition of faster growth of *Y. lipolytica* on nitrate as N-source.
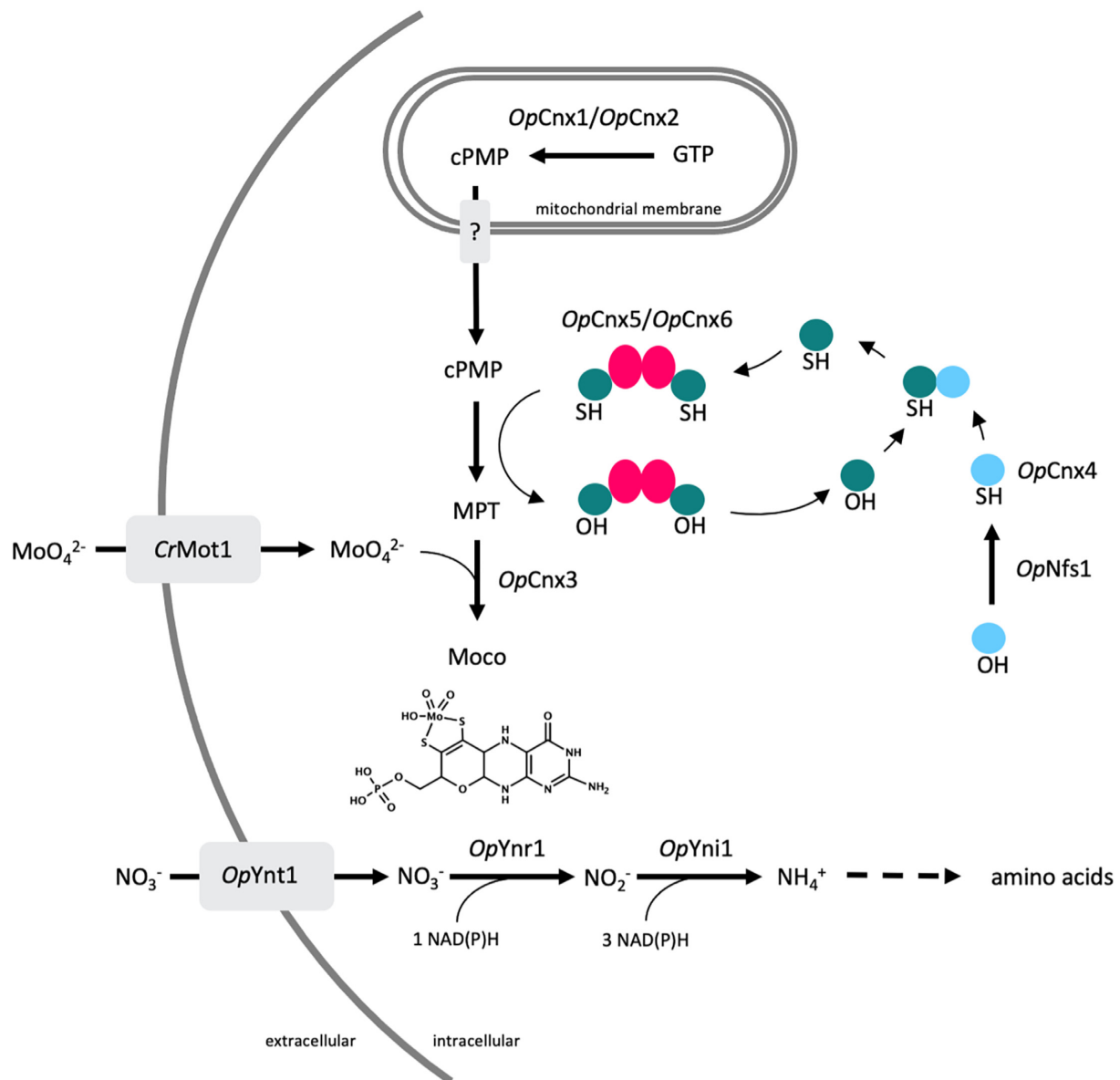
Figure 1. Schematic representation of the Moco biosynthesis pathway coupled to the nitrate assimilation pathway. GTP is converted to cyclic pyranopterin phosphate (cPMP) in the yeast mitochondria by *Op*Cnx1 and *Op*Cnx2. In the cytosol, cPMP is converted to molybdopterin (MPT) by *Op*Cnx5 and *Op*Cnx6. The sulfur moiety on *Op*Cnx5 is restored by *Op*Cnx4 that transfers the sulfur atom obtained by action of the cysteine desulfurase *Op*Nfs1. Molybdate (MoO_4^{2-}) is imported through the high affinity transporter *Cr*Mot1 and is inserted in MPT by *Op*Cnx3 to form Moco. Nitrate is imported via *Op*Ynt1 and reduced by the Moco-dependent nitrate reductase *Op*Ynr1 to nitrite. *Op*Yni1 converts nitrite to ammonia that finally enters the native nitrogen assimilation pathway. *Op*Cnx4, *Op*Cnx5 and *Op*Cnx6 are shown in light blue, teal and magenta, respectively. A question mark indicates a yet unknown cPMP transporter and a dashed line indicates multiple enzymatic steps.

The second gene (YALI0_E24167g) mutated in two different isolates IMS1180 and IMS1177 encoded a putative sulfite transporter that shared similarity to the S. *cerevisiae* sulfite efflux pump Ssu1 (Avram and Bakalinsky 1997). The nature of the mutations found in YALI0_E24167g would suggest a loss of function. In IMS1177 the mutation G743A resulted in the introduction of a stop codon at position 248. Consequently, the mutated protein would be truncated to 45% of the original sequence and thus likely not functional.

The last gene found mutated in two different isolates was *Spcas9*. Although different, these two mutations occurred in a section of the gene encoding amino acids located in the same functional domain. The *Spcas9* mutation in IMS1175 (G2959A)

and in IMS1180 (C3020A) led to amino acids change in the RuvC-III domain of *Sp*Cas9 (Jinek *et al.* 2014).

Whereas IMS1175 and IMS1177 both harbored mutations in *OpCNX1*, interestingly IMS1180 had a mutation in *OpCNX2*. As observed for *OpCNX1*, the *OpCNX2* mutation was located in the 5′ end the gene (G4A).

On top of that, four more mutations were identified in only one isolates, it included YALI0_D25784g encoding a hypothetical protein, YALI0_A04697g a gene encoding a putative serine/threonine protein kinase, YALI0_E00638g a gene encoding a putative methyl citrate synthase in IMS1175 and YALI0_F05346g a gene encoding a protein exhibiting similarity with a cutinase from *Fusarium solani* cutinase.
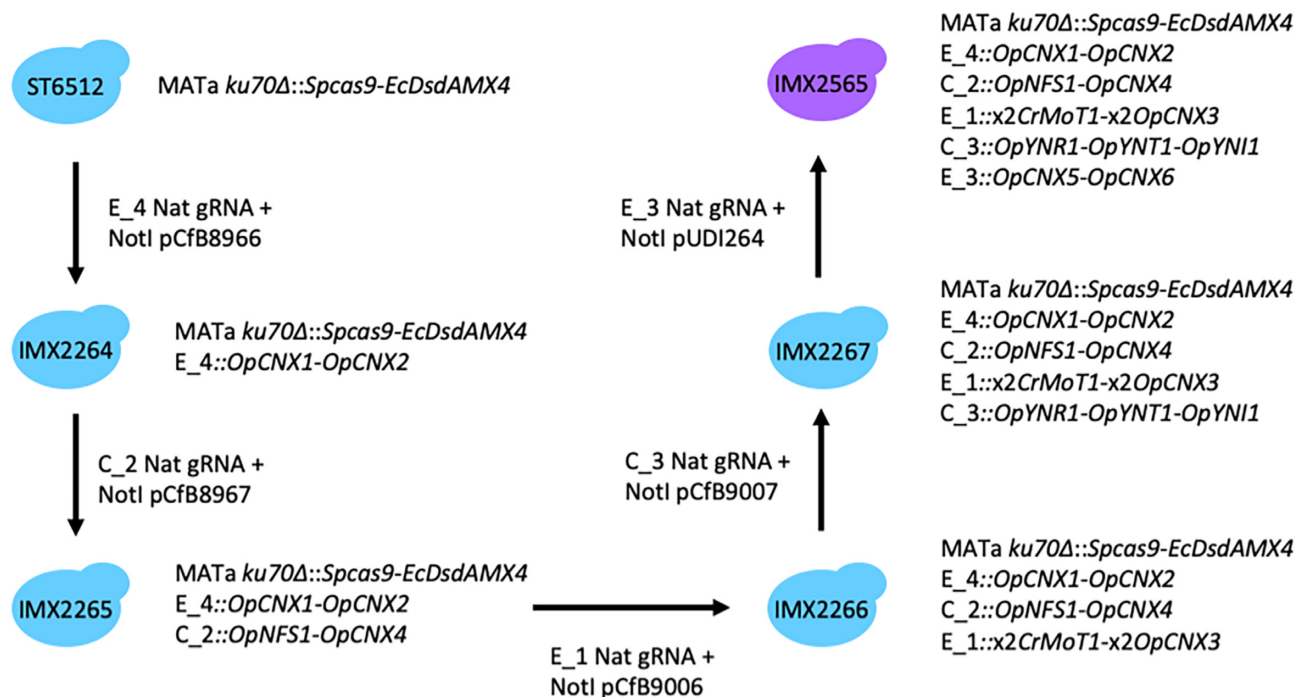
Figure 2. Schematic representation of strain construction. Strain ST6512, which constitutively expresses a *Spcas9*, was sequentially transformed five times with a targeting gRNA plasmid and a NotI-linearized plasmid carrying the integration cassettes as repair fragment, yielding IMX2565. Intermediate strains and the final strain IMX2565 are shown in light-blue and purple, respectively.

ALE for fast growth on nitrate was associated with an increased Moco-dependent nitrate reductase activity

To investigate the effects of the ALE experiment, NADPH- and Moco-dependent nitrate reductase activity was assayed from cell-extracts of single colony isolates IMS1180, IMS1175 and IMS1177, evolved populations 1–2–3 after 50 transfers in SMD_{NO3}, the parental un-evolved engineered strain IMX2565 and the Cas9-expressing parental strain ST6512 (Fig. 4). While as expected, cell extract from ST6512 which does not carry any of the heterologous genes for Moco biosynthesis and nitrate assimilation, showed no significant nitrate reductase activity, the engineered strain IMX2565 showed an activity of 0.004 ± 0.001 μM $NADP^+$/min/mg total protein. Although significant, this activity was up to 55-fold lower than the one observed for the evolved single colony isolates IMS1180, IMS1175 and IMS1177 that reached up to 0.22 ± 0.01 μM $NADP^+$/min/mg total protein. Finally, cell extracts from the evolved populations showed activity values that were comparable for the 335 generations old, prolonged evolution line 1 and within 2-fold for the 335 generations old, prolonged evolution 2 and 3 with those measured for the single colony isolates, reaching up to 0.41 ± 0.03 μM $NADP^+$/min/mg total protein.

To see whether the increase in nitrate reductase activity was associated with improved growth performance on nitrate, the strains ST6512, IMS11780, IMS1175, IMS1177, as well as the prolonged evolved populations at T50 1–2–3 were cultivated in chemically defined medium with nitrate as N-source (SMD_{NO3^-}). The strains were grown in aerobic shake flasks and OD $_{660}$, glucose, nitrate, nitrite and ammonium levels were monitored over time (Fig. 5). As expected, the parental strain ST6512 did not show any growth and/or glucose/nitrate consumption (Fig. 5B). All the other strains and evolved populations showed a growth rate ranging between 0.07 ± 0.01 and 0.16 ± 0.01 h $^{-1}$. Although

slightly different in absolute values when compared to the growth rates measured in 96-wells format (Fig. 3B), the ones measured in 100 mL shake flasks followed the same trend with IMS1180 being the slowest and IMS1175 being the fastest growing isolates, respectively. Growth rate of the evolved populations, that were kept evolving for about 195 generations after single colonies were isolated, was significantly higher when compared to the respective single clones, with up to 2-folds increase (Fig. 5A). Notably, both evolved isolates and further evolved populations excreted moderate amounts of the intermediates nitrite and ammonia during the exponential phase of growth, suggesting that nitrate assimilation was not growth-limiting (Fig. 5C–H). Similarly to what happened to engineered nitrate-assimilating *S. cerevisiae* strains (Perli *et al.* 2021), ammonia and nitrite were also excreted toward the end of the batch fermentation, resulting from continuous conversion or possible cell lysis.

DISCUSSION

Moco-dependent enzymes catalyse many redox reactions involved in the carbon, nitrogen and sulfur cycles (Leimkuhler and Iobbi-Nivol 2016) and might be harnessed to expand substrates range for microbial growth. This study firmly established that although Moco pathway is predominantly absent in Saccharomycotina yeasts, this function can be implemented by metabolic engineering. This study is, after introduction in *S. cerevisiae*, the second successful engineering of the pathway in yeasts. The large phylogenetic distance between the two tested hosts would also suggest that this pathway engineering could be extrapolated to an even larger set of budding yeasts (Shen *et al.* 2018). While in both biological systems functionality through growth coupling with nitrate assimilation required an evolution step, the resulting mutations identified were different. In

(A)

(B)

(C)
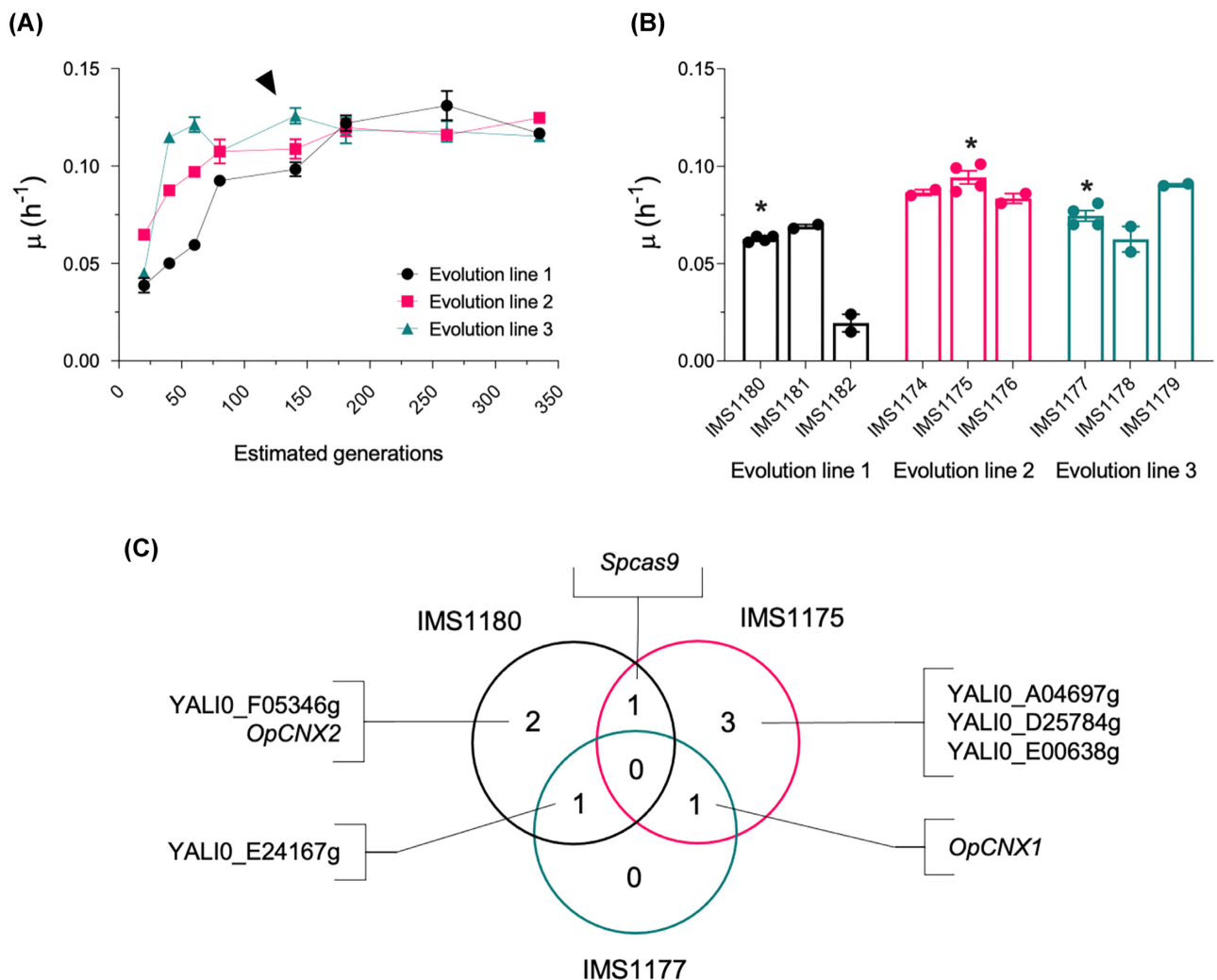
Figure 3. Maximum specific growth rate (μ) values of IMX2565 throughout the adaptive laboratory evolution experiment **(A)**, growth rates of single colony isolates **(B)** on SMD_{NO3} and Venn diagram highlighting genes affected by non-synonymous mutations and/or INDELs in independently evolved isolates IMS1175, IMS1177 and IMS1180 **(C)**. An arrow in panel A indicates the time-point when single colonies were isolated from the three independent evolving populations while asterisks in panel B indicate single colony isolates selected for whole-genome re-sequencing and further characterization. Evolution line 1, 2 and 3 are shown in black, magenta and teal, respectively. Error bars represent the standard error of the mean for replicate cultures ($n = 4$ with the exception of IMS1181, IMS1182, IMS1174, IMS1176, IMS1178 and IMS1179 where $n = 2$). The Venn diagrams shows genes that acquired one or more non-synonymous mutations or INDELs in multiple independent evolution experiments as well as genes that were affected in a single replicate. Apparent mutations also found in the genome of the parent strain ST6512 and/or IMX2565 were subtracted and not shown.

the precedent example in *S. cerevisiae*, adaptation to fast utilization of nitrate involved segmental aneuploidy of the whole heterologous cluster, accompanied with a strong increase of nitrate reductase activity (Perli *et al.* 2021). However, since the increase in copy number affected both genes of the Moco biosynthesis and the nitrate assimilation pathways it was not really possible to discriminate which metabolic branch was the most limiting. In *Y. lipolytica* instead, the results would indicate that Moco synthesis is most limiting. This was supported by the absence of gene dosage but instead by recurrent mutations in the mitochondrial enzymes *OpCnx1* and*OpCnx2* that catalyse the formation of cPMP in the very first step of Moco biosynthesis (Fig. 1). Evolved isolates IMS1175 and IMS1177 carried a mutation in the *OpCnx1* whereas the third isolate IMS1180 carried a mutation in *OpCnx2*. But more specifically, the non-synonymous mutations led to amino acid change in N-terminus of both proteins changing the sequence of the mitochondrial targeting signal.

Although theoretical, the presence of the mutation systematically improved the *in silico* prediction of mitochondrial targeting likelihood using five different algorithms (Small *et al.* 2004; Petsalaki *et al.* 2006; Fukasawa *et al.* 2015; Almagro Armenteros *et al.* 2017, 2019; Table 5). These mutations could contribute to improve OpCnx1 and 2 translocations into the organelle and optimize the supply of cPMP for Moco biosynthesis. The higher Moco availability would then be at the origin of the massive increase by 1 to 2 order of magnitude of nitrate reductase activity (Fig. 4). These results seem to indicate that although the *O. parapolymorpha* biosynthetic genes are sufficient to implement the synthesis of the new cofactor in other yeast species, the adaptation required to tune its supply optimally might be species dependent.

Among the three genes that were mutated in at least two isolates we found YALI0_E24167g (mutated in IMS1177 and IMS1180), a protein containing a predicted SLAC1 domain

Table 4. SNVs and INDELs found in single colony isolates IMS1775, IMS1177 and IMS1180 obtained from the serial transfer evolution experiment of strain IMX2565 in SMD$_{NO3}$.

Mutated gene	Mutation type	Base change	Amino acid change	Gene annotation
IMS1175				
YALI0_A04697g	INDEL	T970TG	Gln324Frameshift	Similar to uniprot|O42626 *Neurospora crassa* Serine/threonine-protein kinase nrc-2 (Nonrepressible conidiation protein 2)
YALI0_D25784g	SNV	T457C	Ser151Pro	weakly similar to uniprot|O74782 *Schizosaccharomyces pombe* Hypothetical protein
YALI0_E00638g	SNV	G868T	Gly290Cys	Similar to uniprot|Q9TEM3 *Emericella nidulans* MCSA Methylcitrate synthase precursor
*Op*CNX1	SNV	G22A	Glu8Lys	GTP 3',8-cyclase
*Sp*cas9	SNV	G2959A	Ala987Thr	CRISPR-associated endonuclease Cas9
IMS1177				
YALI0_E24167g	SNV	G743A	Trp248Stop	Weakly similar to uniprot|Q2VQ77 *Saccharomyces cerevisiae* YPL092w *SSU1* Plasma membrane sulfite pump and required for efficient sulfite efflux
*Op*CNX1	SNV	G22A	Glu8Lys	GTP 3',8-cyclase
IMS1180				
YALI0_E24167g	SNV	A440G	His147Arg	Weakly similar to uniprot|Q2VQ77 *Saccharomyces cerevisiae* YPL092w *SSU1* Plasma membrane sulfite pump and required for efficient sulfite efflux
YALI0_F05346g	SNV	G337A	Ala113Thr	Weakly similar to uniprot|Q00858 *Fusarium solani* cutinase gene palindrome-binding protein
*Op*CNX2	SNV	G4A	Val2Met	Cyclic pyranopterin monophosphate synthase
*Sp*cas9	SNV	C3020A	Ala1007Asp	CRISPR-associated endonuclease Cas9

Table 5. Likelihood of mitochondrial targeting in WT and mutated OpCnx1-OpCnx2 protein sequences across different prediction tools.

Prediction tool	*Op*Cnx1		*Op*Cnx2	
	WT	Mutated	WT	Mutated
TargetP 2.0	0.000208	0.000649	0.000525	0.001879
DeepLoc 1.0	0.0875	0.1946	0.1252	0.1261
MitoFates	0.080	0.280	0.000	0.000
Predotar	0.01	0.14	0.00	0.00
PredSL	0.006826	0.097417	0.004088	0.004091

characteristic of voltage-dependent anion transporters such as nitrate and sulfite exporters (Vahisalu *et al.* 2008). The protein is similar to the *S. cerevisiae* sulfite transporter Ssu1 which has been previously shown to be able to also export nitrate and nitrite (Cabrera *et al.* 2014). While the IMS1180 mutation in YALI0_E24167g led to an His to Arg change, the mutation found in strain IMS1177 introduced a stop codon (Trp248Stop), creating a truncation of the translation product by 180 amino acids, representing 45% of the protein length, that included not fewer than four transmembrane domains that undoubtedly caused
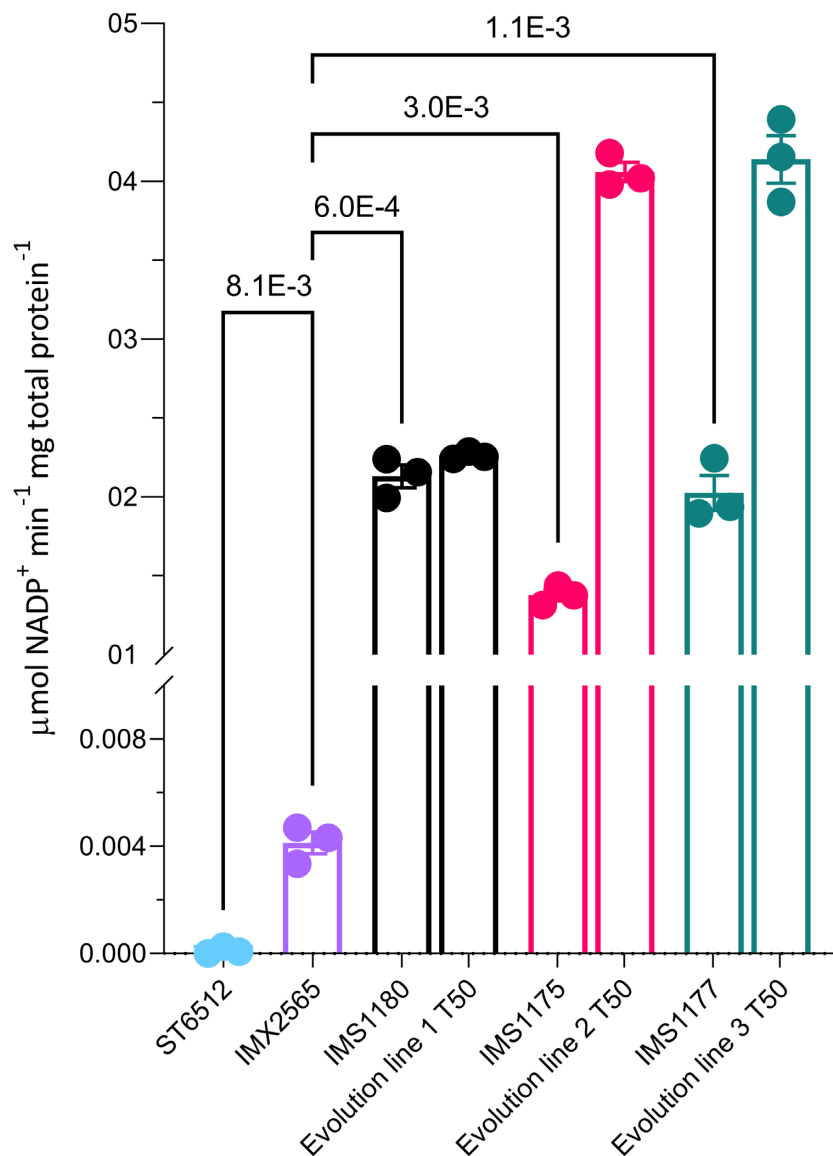
Figure 4. NADPH-dependent nitrate reductase activity measured from cell extracts. ST6512, IMX2565, isolate IMS1180 and evolution line 1 at T50, isolate IMS1175 and evolution line 2 at T50 and isolate IMS1177 and evolution line 3 at T50 are shown in light blue, purple, black, magenta and teal, respectively. Cell extract was prepared from 100 mL of stationary phase cell cultures in SMD_{urea} for ST6512, IMX2565, IMS1180, IMS1175 and 1177 and in SMD_{NO3} for evolution lines T50 1, 2 and 3. P-values for two-tailed Welch's t-test are shown above the tested pairs. Error bars represent the standard error of the mean of technical replicates ($n = 3$).

a loss of function. Assuming that YALI0_E24167g shared function with its *S. cerevisiae* ortholog, the loss of function might represent a mechanism to avoid nitrogen loss through excessive nitrite export; it is worth noticing that this transport system would not be the only one as moderate extracellular nitrite concentration could still be measured. Maintenance of a higher intracellular nitrite could also partially explain the increase in nitrate assimilation and growth rate after evolution in nitrate-containing medium.

Interestingly, the third gene that was affected by non-synonymous mutations in at least two isolates (IMS1175 and IMS1180), was *Spcas9*. Although resulting in amino acid changes, it is not obvious to predict the impact of the mutations on the endonuclease activity. However, both mutations (Ala987Thr and Ala1007Asp) were found in the RuvC-III nuclease domain of Cas9

protein that extends from 925 to 1101. Several other mutations in RuvC-III at position 982, 983 and 986 have been described (Nishimasu *et al.* 2014) and all yielded either a decrease or an alteration of the endonuclease activity resulting in mutants able to only cleave one strand instead of two (Fonfara *et al.* 2014; Jinek *et al.* 2014). This was confirmed experimentally, as our attempts to further engineer the evolved isolates systematically failed. We cannot exclude that recurrent mutagenesis of Cas9 might take place to counteract potential endonuclease toxicity.

The Moco platform strain constructed and characterized in this study represents a stepping stone towards the exploitation of a new class of enzymes that might contribute to expand the metabolic capabilities of yeast microbial cell factories by enabling new metabolic engineering strategies.
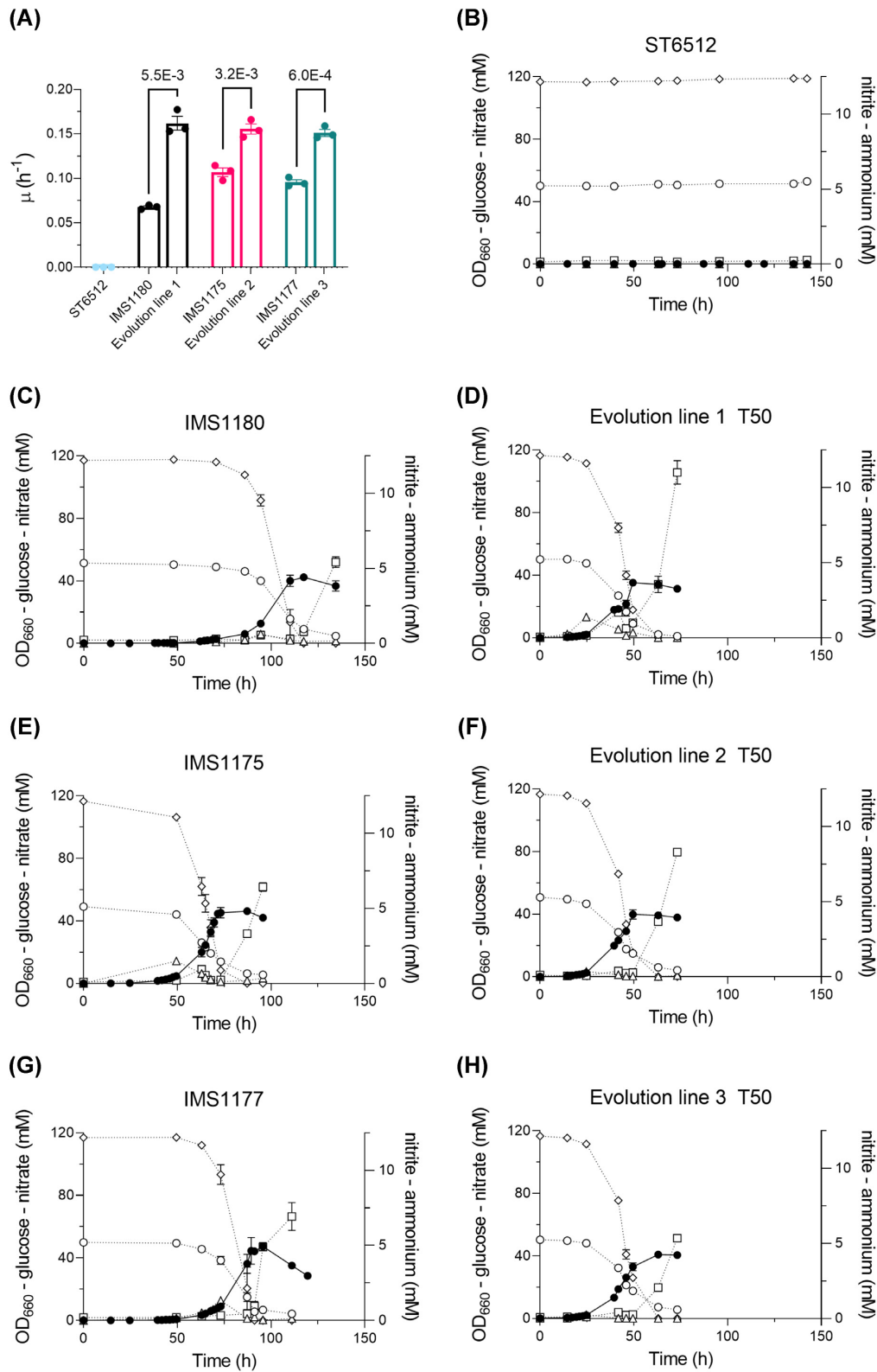
Figure 5. Growth rates **(A)** and growth curves of ST6512 **(B)**, IMS1180 **(C)**, evolution line 1 T50 **(D)**, IMS1175 **(E)**, evolution line 2 T50 **(F)**, IMS1177 **(G)** and evolution line 3 T50 **(H)** on SMD$_{NO3}$. Symbols indicate biomass (●), glucose (◊), nitrate (○), nitrite (□) and ammonium (△). Statistical analysis was based on a two-tailed Welch's *t*-test and P-values are reported for tested pairs. Error bars represent the standard error of the mean for replicate cultures (*n* = 3).

SUPPLEMENTARY DATA

FUNDING

AUTHOR CONTRIBUTIONS

TP and JMD designed the experiments and wrote a first version of the manuscript. All authors critically read this version, provided input and approved the final version. TP performed the experiments and analysed the genome sequence data.

ACKNOWLEDGMENTS

REFERENCES

Almagro Armenteros JJ, Salvatore M, Emanuelsson O *et al.* Detecting sequence signals in targeting peptides using deep learning. *Life Sci Allian* 2019;**2**:e201900429.

Almagro Armenteros JJ, Sonderby CK, Sonderby SK *et al.* DeepLoc: prediction of protein subcellular localization using deep learning. *Bioinformatics* 2017;**33**:3387–95.

Andersen JB, Sternberg C, Poulsen LK *et al.* New unstable variants of green fluorescent protein for studies of transient gene expression in bacteria. *Appl Environ Microbiol* 1998;**64**:2240–6.

Arnesen JA, Kildegaard KR, Cernuda Pastor M *et al. Yarrowia lipolytica* strains engineered for the production of terpenoids. *Front Bioeng Biotechnol* 2020;**8**:945.

Avram D, Bakalinsky AT. *SSU1* encodes a plasma membrane protein with a central role in a network of proteins conferring sulfite tolerance in *Saccharomyces cerevisiae. J Bacteriol* 1997;**179**:5971–4.

Barth G, Gaillardin C. Physiology and genetics of the dimorphic fungus *Yarrowia lipolytica. FEMS Microbiol Rev* 1997;**19**:219–37.

Bitinaite J, Rubino M, Varma KH *et al.* USER friendly DNA engineering and cloning method by uracil excision. *Nucleic Acids Res* 2007;**35**:1992–2002.

Blazeck J, Hill A, Jamoussi M *et al.* Metabolic engineering of *Yarrowia lipolytica* for itaconic acid production. *Metab Eng* 2015;**32**:66–73.

Broderick JB. *Coenzymes and Cofactors.* Chichester: John Wiley & Sons, Ltd, 2001.

Cabrera E, Gonzalez-Montelongo R, Giraldez T *et al.* Molecular components of nitrate and nitrite efflux in yeast. *Eukaryot Cell* 2014;**13**:267–78.

Champe PC, Harvey RA, Ferrier DR. *Biochemistry.* Philadelphia, PA: Lippincott Williams & Wilkins, 2005.

Chen DC, Beckerich JM, Gaillardin C. One-step transformation of the dimorphic yeast *Yarrowia lipolytica. Appl Microbiol Biotechnol* 1997;**48**:232–5.

Cingolani P, Platts A, Wang le L *et al.* A program for annotating and predicting the effects of single nucleotide polymorphisms, SnpEff: sNPs in the genome of *Drosophila melanogaster* strain w1118; iso-2; iso-3. *Fly* 2012;**6**:80–92.

Cvetkovic A, Menon AL, Thorgersen MP *et al.* Microbial metalloproteomes are largely uncharacterized. *Nature* 2010;**466**: 779–82.

Danecek P, Auton A, Abecasis G *et al.* The variant call format and VCFtools. *Bioinformatics* 2011;**27**:2156–8.

Dujon B, Sherman D, Fischer G *et al.* Genome evolution in yeasts. *Nature* 2004;**430**:35–44.

Fischer K, Llamas A, Tejada-Jimenez M *et al.* Function and structure of the molybdenum cofactor carrier protein from *Chlamydomonas reinhardtii. J Biol Chem* 2006;**281**:30186–94.

Fonfara I, Le Rhun A, Chylinski K *et al.* Phylogeny of Cas9 determines functional exchangeability of dual-RNA and Cas9 among orthologous type II CRISPR-Cas systems. *Nucleic Acids Res* 2014;**42**:2577–90.

Fukasawa Y, Tsuji J, Fu SC *et al.* MitoFates: improved prediction of mitochondrial targeting sequences and their cleavage sites. *Mol Cell Proteomics* 2015;**14**:1113–26.

Galanie S, Thodey K, Trenchard IJ *et al.* Complete biosynthesis of opioids in yeast. *Science* 2015;**349**:1095–100.

Germann SM, Baallal Jacobsen SA, Schneider K *et al.* Glucose-based microbial production of the hormone melatonin in yeast *Saccharomyces cerevisiae. Biotechnol J* 2016;**11**:717–24.

Gibson DG, Young L, Chuang RY *et al.* Enzymatic assembly of DNA molecules up to several hundred kilobases. *Nat Methods* 2009;**6**:343–5.

Hille R, Hall J, Basu P. The mononuclear molybdenum enzymes. *Chem Rev* 2014;**114**:3963–4038.

Hille R. Molybdenum and tungsten in biology. *Trends Biochem Sci* 2002;**27**:360–7.

Holkenbrink C, Dam MI, Kildegaard KR *et al.* EasyCloneYALI: cRISPR/Cas9-based synthetic toolbox for engineering of the yeast *Yarrowia lipolytica. Biotechnol J* 2018;**13**:e1700543.

Holkenbrink C, Ding BJ, Wang HL *et al.* Production of moth sex pheromones for pest control by yeast fermentation. *Metab Eng* 2020;**62**:312–21.

Inoue H, Nojima H, Okayama H. High efficiency transformation of *Escherichia coli* with plasmids. *Gene* 1990;**96**:23–8.

Iobbi-Nivol C, Leimkuhler S. Molybdenum enzymes, their maturation and molybdenum cofactor biosynthesis in *Escherichia coli. Biochim Biophys Acta Bioenerg* 2013;**1827**:1086–101.

Jinek M, Jiang F, Taylor DW *et al.* Structures of Cas9 endonucleases reveal RNA-mediated conformational activation. *Science* 2014;**343**:1247997.

Kerscher S, Durstewitz G, Casaregola S *et al.* The complete mitochondrial genome of *Yarrowia lipolytica. Comp Funct Genomics* 2001;**2**:80–90.

Leimkuhler S, Buhning M, Beilschmidt L. Shared sulfur mobilization routes for tRNA thiolation and molybdenum cofactor biosynthesis in prokaryotes and eukaryotes. *Biomolecules* 2017;**7**:5.

Leimkuhler S, Iobbi-Nivol C. Bacterial molybdoenzymes: old enzymes for new purposes. *FEMS Microbiol Rev* 2016;**40**:1–18.

Li Y, Smolke CD. Engineering biosynthesis of the anticancer alkaloid noscapine in yeast. *Nat Commun* 2016;**7**:12137.

Looke M, Kristjuhan K, Kristjuhan A. Extraction of genomic DNA from yeasts for PCR-based applications. *BioTech* 2011;**50**:325.

Marella ER, Dahlin J, Dam MI *et al*. A single-host fermentation process for the production of flavor lactones from non-hydroxylated fatty acids. *Metab Eng* 2020;**61**:427–36.

Mendel RR. The molybdenum cofactor. *J Biol Chem* 2013;**288**:13165–72.

Milne N, Luttik MAH, Cueto Rojas HF *et al*. Functional expression of a heterologous nickel-dependent, ATP-independent urease in *Saccharomyces cerevisiae*. *Metab Eng* 2015;**30**:130–40.

Nijkamp JF, van den Broek MA, Geertman JM *et al*. De novo detection of copy number variation by co-assembly. *Bioinformatics* 2012;**28**:3195–202.

Nishimasu H, Ran FA, Hsu PD *et al*. Crystal structure of Cas9 in complex with guide RNA and target DNA. *Cell* 2014;**156**: 935–49.

Perli T, van der Vorm DA, Wassink M *et al*. Engineering heterologous molybdenum-cofactor-biosynthesis and nitrate-assimilation pathways enables nitrate utilization by Saccharomyces cerevisiae. *Metab Eng* 2021;**65**: 11–29.

Perli T, Vos AM, Bouwknegt J *et al*. Identification of oxygen-independent pathways for pyridine-nucleotide and Coenzyme-A synthesis in anaerobic fungi by expression of candidate genes in yeast. *bioRxiv* 2020. DOI: 10.1128/mBio.00967-21.

Petsalaki EI, Bagos PG, Litou ZI *et al*. PredSL: a tool for the N-terminal sequence-based prediction of protein subcellular localization. *Genomics Proteomics Bioinformatics* 2006;**4**: 48–55.

Rajagopalan KV, Johnson JL. The pterin molybdenum cofactors. *J Biol Chem* 1992;**267**:10199–202.

Ratledge C. Regulation of lipid accumulation in oleaginous micro-organisms. *Biochem Soc Trans* 2002;**30**:1047–50.

Ravin NV, Eldarov MA, Kadnikov VV *et al*. Genome sequence and analysis of methylotrophic yeast *Hansenula polymorpha* DL1. *BMC Genomics* 2013;**14**:837.

Rumelhard M, Hosako H, Eurlings IM *et al*. Safety evaluation of rebaudioside A produced by fermentation. *Food Chem Toxicol* 2016;**89**:73–84.

Shen XX, Opulente DA, Kominek J *et al*. Tempo and mode of genome evolution in the budding yeast subphylum. *Cell* 2018;**175**:1533–45.

Small I, Peeters N, Legeai F *et al*. Predotar: a tool for rapidly screening proteomes for N-terminal targeting sequences. *Proteomics* 2004;**4**:1581–90.

Solis-Escalante D, Kuijpers NG, Bongaerts N *et al*. amdSYM, a new dominant recyclable marker cassette for Saccharomyces cerevisiae. *FEMS Yeast Res* 2013;**13**:126–39.

Tejada-Jimenez M, Llamas A, Sanz-Luque E *et al*. A high-affinity molybdate transporter in eukaryotes. *Proc Natl Acad Sci* 2007;**104**:20126–30.

Tsugawa R, Nakase T, Kobayash T *et al*. Fermentation of *n*-paraffins by yeast .3. alpha-Ketoglutarate productivity of various yeast. *Agr Biol Chem Tokyo* 1969;**33**:929.

Vahisalu T, Kollist H, Wang YF *et al*. SLAC1 is required for plant guard cell S-type anion channel function in stomatal signalling. *Nature* 2008;**452**:487–91.

Verduyn C, Postma E, Scheffers WA *et al*. Effect of benzoic acid on metabolic fluxes in yeasts: a continuous-culture study on the regulation of respiration and alcoholic fermentation. *Yeast* 1992;**8**:501–17.

Verhoeven MD, Lee M, Kamoen L *et al*. Mutations in *PMR1* stimulate xylose isomerase activity and anaerobic growth on xylose of engineered *Saccharomyces cerevisiae* by influencing manganese homeostasis. *Sci Rep-Uk* 2017;**7**:46155.